Single Molecule Interactions at a Surfactant-Modified H_2 Surface Nanobubble

Milomir Suvira and Bo Zhang*
Department of Chemistry, University of Washington, Seattle, WA 98195-1700 United States

Corresponding author, email; zhangb@uw.edu

Phone 1-206-543-1767

Fax: 1-206-686-8665

Abstract

In schematics and cartoons, the gas-liquid interface is often drawn as solid lines that aid to distinguish the separation of the two phases. However, on the molecular level, the structure, shape, and size of the gas-liquid interface remains elusive. Furthermore, the interactions of molecules at gas-liquid interfaces must be considered in various contexts including atmospheric chemical reactions, wettability of surfaces, and numerous other relevant phenomena. Hence, understanding the structure and interactions of molecules at the gas-liquid interface is critical to further improve technologies that operate between the two phases. Electrochemically generated surface nanobubbles provide a stable, reproducible, and high-throughput platform for the generation of a nanoscale gas-liquid boundary. We use total internal reflection fluorescence microscopy (TIRF) to image single fluorophore labeling of surface nanobubbles in the presence of surfactant. The accumulation of surfactant on the nanobubble surface changes the interfacial properties of the gas-liquid interface. The single molecule approach reveals that fluorophore adsorption and residence lifetime at the interface is greatly impacted by the charge of the surfactant layer at the bubble surface. We demonstrate that the fluorescence readout is either short or long-lived depending on the repulsive or attractive environment between fluorophores and surfactants. Additionally, we investigated the effect of surfactant chain length and salt type/concentration on fluorophore lifetime at the nanobubble surface.

Introduction

The boundary between the gas and liquid phase can be found in numerous places in the natural world. Many key processes in atmospheric and environmental chemistry, such as the adsorption, solvation, and reactivity of gases and small organic molecules, take place at the surface of atmospheric aerosols and water surfaces. In chemistry, the air-water interface has been shown to exhibit unique interfacial properties that yield significantly accelerated reaction rates compared to bulk water ('on-water' catalysis).[1-4] Nonetheless, the orientation and structural arrangement of water molecules and other species such as surfactant at the gas-liquid interface continues to be a topic of debate.[5-9]

Gas containing surface nanobubbles provide a unique opportunity to study the gas-liquid interface at the nanoscale. Surface nanobubbles are readily generated using organic solvent exchange[10,11] and electrochemistry[12,13]. These gaseous entities have garnered a significant amount of attention due to their mysterious stability[14] and implications in electrochemical processes[15]. Several recent reviews detail the current understanding and unresolved questions on surface nanobubbles.[16,17] Nanobubbles have been studied using a wide range of analytical tools including atomic force microscopy (AFM)[18], nano-electrochemistry[19], surface plasmon resonance imaging[20], synchrotron-based transmission x-ray microscopy[21], scanning electrochemical cell microscopy (SECCM)[22], interface reflection microscopy[23], and fluorescence-based imaging[24,25]. Although these studies have provided tremendous insight into the nucleation, growth, stability, and physical characteristics of surface nanobubbles, the nature of the gas-liquid interface has been essentially unexplored.

Early AFM images revealed that surface nanobubbles come in different shapes and sizes.[26] Presumably, each nanobubble has unique interfacial properties that likely differ from their microscopic or macroscopic counterparts. Exploring the heterogeneity of a bubble population is necessary to gain a more complete understanding of surface nanobubbles. Super resolution microscopy is a powerful tool for studying surface nanobubbles as it allows one to use single fluorophore molecules to label many bubbles on the surface of a transparent electrode and image them with exceedingly high spatial resolution. Such measurements can allow us to probe certain bubble characteristics including size, nucleation rate, and

growth.[27] During our investigation of nanobubble nucleation in the presence of surfactant, we noticed that the lifetime and intensity of the labeling fluorophore at surfactant-coated nanobubbles were drastically different from "clean" nanobubbles.[28] Although fluorophore interaction at biological targets has been investigated, the governing phenomenon affecting fluorophore interaction at the gas-liquid interface of a surface nanobubble remains largely unknown.[29] Furthermore, we recognized the unique opportunity to probe single fluorophore dynamics via systematic changes to the gas-liquid interface through the adsorption of surfactants with different charges, hydrophobicities, surface activities, and other chemical properties.

Herein, we demonstrate that the fluorophore and surfactant charge greatly alter the degree of interaction at the bubble surface due to attractive or repulsive electrostatic forces between opposite and same charge molecules. Furthermore, the contrast between fluorophore and surfactant adsorption/desorption kinetics at the gas-liquid interface appears to dictate whether a change in fluorophore lifetime is observed. Finally, we probe the effect of salt concentration and type on fluorophore residence at the surfactant modified bubble surface.

Experimental Section

Chemicals and materials: R6G perchlorate (Kodak), sulforhodamine g (Sigma-Aldrich), sodium sulfate (J.T. Baker), magnesium sulfate (Sigma-Aldrich), sodium nitrate (Sigma-Aldrich), isopropyl alcohol (Fisher Chemical), sodium dodecyl sulfate (SDS) (Sigma-Aldrich), cetrimonium bromide (16TAB) (Sigma-Aldrich), myristyltrimethylammonium bromide (14TAB) (Sigma-Aldrich), dodecyltrimethylammonium bromide (12TAB) (Sigma-Aldrich), indium-tin oxide (ITO)-coated coverslips (SPI supplies). All solutions were made using deionized water (>18 MΩ•cm). All chemicals were used exclusively for single molecule experiments in order to avoid potential fluorescent contamination from other sources. All chemicals are at least ≥ 98% pure. Control experiments were readily conducted to ensure chemical purity. The critical micelle concentration used for the percent

concentration calculation for SDS, 16TAB, 14TAB, and 12TAB is 8.3, 0.96, 4.5, and 15.9 mM, respectively.[30]

TIRF Microscopy: Objective-based total internal reflection fluorescence (TIRF) microscopy was performed using an inverted microscope (Olympus). An Olympus Apo N 60X 1.49 NA oil objective with an additional 1.5X magnification source was used to generate an evanescent wave at the ITO working electrode using a 532 nm laser (15 mW) as the excitation light source (CrystaLaser). The excitation and emission light were filtered using an ET590/50m filter (Chroma Technology). An Andor iXon+ EMCCD camera set with a preamplifier of 5.1 and gain amplifier of 300 were used for all imaging experiments. The camera frame rate was set to 50 ms (19.81 Hz) unless otherwise noted. A 6 µL droplet of solution containing 100 pM fluorophore, varying concentration/type of salt, and varying concentration/type of surfactant were placed on a 2 mm diameter hole cut in a polydimethylsiloxane (PDMS) film defining the ITO working electrode. All labeling experiments were recorded for 500 frames (25 s). To generate surface nanobubbles, a potentiostat (Bipotentiostat AFCBP1, Pine) was used to apply a constant -1 V to the ITO working electrode with a Pt wire acting as a quasi-reference electrode (QRE). Amperometry traces were recorded at a 50 Hz sampling frequency using a MiniDigi 1A digitizer (Axon Instruments) interfaced with the Axoscope 10.4 software (Molecular Devices).

Image Analysis and Single-Molecule Tracking: The ThunderSTORM plugin in ImageJ was used to obtain the average number of detections per frame.[31] All images were background subtracted using a 5-pixel rolling ball radius. A peak intensity threshold 1.25 times the standard deviation of the wavelet filter was used to fit selected detection spots with a 2D Gaussian function. The TrackMate plugin in ImageJ was used for "spot" tracking.[32] A Laplacian of a Gaussian detector was used to define detect spots above a user set threshold. Once spots were identified, a simple LAP tracker was used to track the duration of the fluorescent spot. The linking and gap-closing distance was set to 300 nm. A gap-closing max frame gap of 3 frames was used. A histogram of the lifetime of detected events was created and fit using a single

exponential decay function in Origin in order to extract τ. An example of the fitting procedure is provided in supplementary information (**Figure S6**).

Results and Discussion

Single molecule labeling of surface nanobubbles. Individual H_2 surface nanobubbles are generated on an optically transparent indium-tin oxide (ITO) working electrode (**Figure 1A**). A platinum wire acts as a quasi-reference electrode (Pt QRE) for which water oxidation is presumably the dominant reference reaction: $2H_2O \rightarrow 4H^+ + 4e^- + O_{2\,(g)}$.[28] Hence, the thermodynamic potential for water reduction, $2H_2O + 2e^- \rightarrow H_{2(g)} + 2OH^-$, occurs on the ITO electrode at -1.23 V vs Pt QRE. After applying a sufficient voltage at the electrode, the accumulation of free H_2 gas at the surface reaches a saturated concentration favorable for heterogeneous nanobubble nucleation.[33] As all experiments are performed at constant potential (-1 V vs Pt QRE), the nanobubble becomes stabilized at the surface when an equilibrium between H_2 gas influx and outflux from the bubble is established.[34-36] The dynamic equilibrium model for explaining nanobubble stability assumes that the size of the nanobubble remains constant at equilibrium.

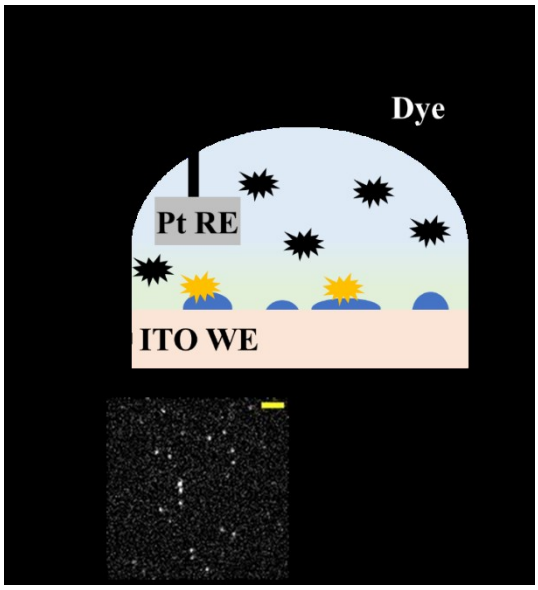

Figure 1: Nanobubble imaging with Total Internal Reflection Fluorescence Microscopy (TIRFM). **A)** Experimental schematic for single fluorophore labeling of electrochemically generated surface nanobubbles. **B)** A typical TIRF image showing H_2 fluorescently-labeled nanobubbles. The scale bar is 3 μm. **C)** time-intensity traces for two randomly selected nanobubbles labeling events shown in **B)** (0.5s vs 100 counts).

A decaying evanescent wave is generated at the ITO surface through objective-based total internal reflection (**Figure 1A**). Once a bubble is generated, fluorophores in solution non-specifically adsorb to the surface of the bubble yielding single fluorescence spots as shown in **Figure 1B**. Nanobubbles (spots) are not detected until the appropriate voltage for H_2 generation is applied. Each "spot" has a characteristic lifetime and intensity that provides information about the nanobubble (**Figure 1C**). For example, the intensity of the fluorophore was used to estimate the height of a surface nanobubble by determining the corresponding position of the fluorophore within the evanescent wave.[27] Finally, the step like nature in the time-intensity trace is indicative of single fluorophores transiently adsorbing onto and desorbing from the bubble surface (**Figure 1C**). A more detailed experimental procedure is provided elsewhere.[27]

In our previous work, we demonstrated that surfactants at the nanobubble surface alter the nature of fluorophore adsorption.[28] In this report, we aim to provide a more detailed understanding of fluorophore interaction at the surfactant modified gas-liquid interface. All experiments were conducted using surfactant concentrations as a function of percent critical micelle concentration (CMC); **Table S1** details the absolute concentration at any given percent CMC.

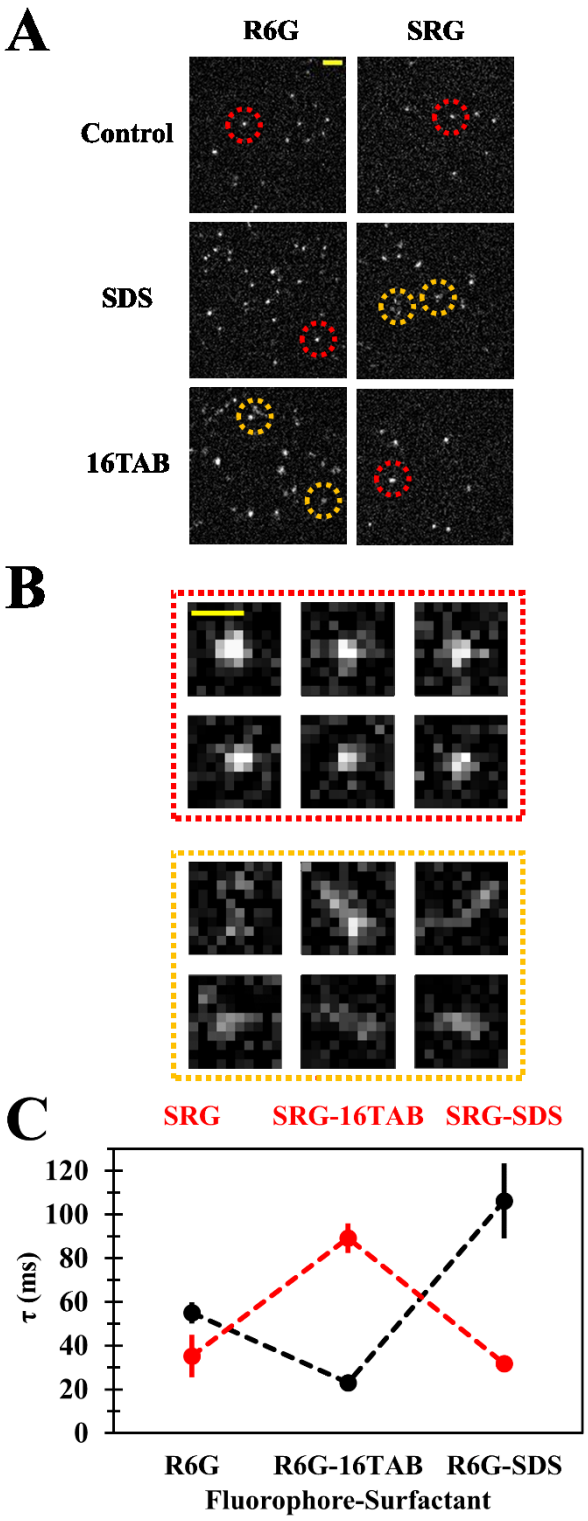

Figure 2: Fluorophore labeling of surfactant stabilized nanobubbles. **A)** Images showing R6G and SRG fluorophore labeling of SDS and 16TAB stabilized nanobubbles. Scale bar is 3 µm. **B)** Representative zoomed in images of "red" and "gold" circles. Scale bar is 1 µm. **C)** Average R6G and SRG residence lifetime at SDS and 16TAB nanobubbles, respectively. The solution contained 100 pM fluorophore, 1 M Na_2SO_4, and 0.05 CMC surfactant. N=5 for each condition. Error bars represent one standard deviation from the mean.

The control panel in **Figure 2A** shows typical images obtained when labeling "clean" nanobubbles using positively charged rhodamine 6G (R6G) and negatively charged sulforhodamine G (SRG). The dye structures are provided in **Figure S1**. Interestingly, we observe a drastically altered optical response between R6G and SRG when attempting to label nanobubbles containing the anionic surfactant sodium dodecyl sulfate (SDS) in solution. First, the nature of the fluorescence response is different. The red circles and representative zoomed in images (**Figure 2B**) exemplify typical fluorescent spots that have a very well-defined circular shape indicative of a single point light emitter. This type of response is seen in the fluorophore control and the R6G-SDS condition. On the other hand, poorly defined fluorescence points are observed when labeling SDS coated nanobubbles with SRG. These labeling events are characteristically low in intensity and have unusual shapes (**Figure 2B**). Surprisingly, the observed phenomenon appears to flip when using R6G and SRG to label nanobubbles with the cationic surfactant cetrimonium bromide, CTAB, present in solution (**Figure 2A**). We refer to CTAB as 16TAB in the present work as it defines the number of carbons in the hydrophobic chain. Labeling experiments without an applied potential (open circuit potential) show few detectable events (**Figure S2**). This suggests that the surfactant molecules are in fact at the bubble surface as opposed to being pre-absorbed onto the ITO electrode before bubble generation.

In order to gain a more quantitative understanding of these "unusual" images, we employed nanobubble spot tracking to extract the lifetime of the nanobubble-fluorophore interaction. This was done by creating histograms of fluorophore lifetime at a bubble surface and then using a single-exponential decay fit to extract the time constant τ.[37,38] An example histogram and decay fit is provided in the supplementary information (**Figure S6**). Note, the residence time of the fluorophore represents adsorption/desorption (on/off) from the bubble surface rather than an extinction of fluorophore emission (ie. photobleaching).[27] We use the word 'lifetime' interchangeably throughout this work to describe the adsorption/desorption processes at the bubble surface. As previously reported, the R6G lifetime at the nanobubble surface increases roughly from 55 ms in the control to 105 ms in the SDS condition (**Figure 2C**).[28] Yet, in the R6G-16TAB condition, the lifetime of the fluorophore at the bubble surface decreases

to 20 ms. The opposite effect, albeit less extreme, is seen in the SRG labeling condition (**Figure 2C**). It is also worth mentioning that the lifetime values presented for the R6G-16TAB and SRG-SDS conditions are overestimations as defining these "unusual spots" becomes challenging during data analysis; we assume that these interactions are even more short-lived than we determined using τ. The nature and lifetime of nanobubble labeling in these experiments is readily apparent in the raw optical readout (**Video S1**).

We believe that the aforementioned results can be explained by favorable and unfavorable fluorophore interactions at the bubble surface. Specifically, it appears that the nature and lifetime of nanobubble labeling is affected by electrostatics. First, the increased lifetime in the R6G-SDS and SRG-16TAB condition can be explained by attractive electrostatic forces between opposite fluorophore-surfactant charges. In other words, the accumulation of anionic and cationic surfactant at the gas-liquid interface increases the interaction between positively (R6G) and negatively (SRG) charged dyes, respectively. Indeed, favorable ion pairing between the negatively charged dye, sunset yellow (SSY), and 16TAB was previously observed in foams.[39] In the same charge condition, R6G-16TAB and SRG-SDS, electrostatic repulsion at the nanobubble surface appears to dominate the nature of nanobubble labeling; so, a short-lived interaction is observed. A simple schematic outlining our hypothesis is presented in **Figure 3A**.

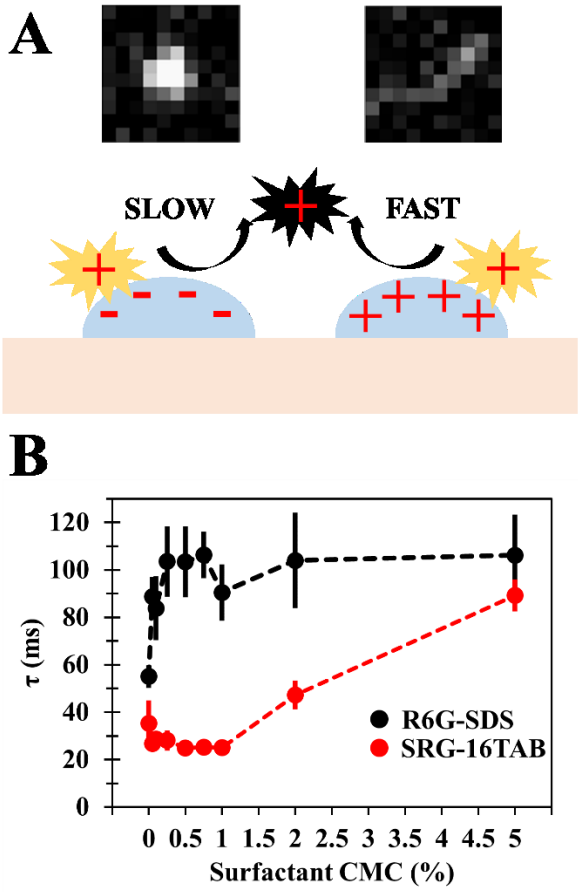

Figure 3: Fluorophore labeling of surfactant stabilized nanobubbles. **A)** Tentative hypothesis. The plus and minus sign denote the charge of the molecule in the labeling experiment. The burst in yellow represents the fluorophore while the plus or minus charge at the blue bubble represents the surfactants at the gas-liquid interface. The fluorescent output (image and lifetime) changes due to attractive or repulsive forces between fluorophores and surfactants **B)** Average R6G and SRG residence lifetime at SDS and 16TAB nanobubbles, respectively. The solution contained 100 pM fluorophore, 1 M Na_2SO_4, and respective surfactant concentration. N=5 for each condition. Error bars represent one standard deviation from the mean.

Lastly, throughout our interpretation of the phenomenon, we have assumed that the bubble size and shape is unchanged in any given condition due to a steady state between gas influx and outflux. We make this assumption because the experiments are done at constant potential (-1 V vs Pt QRE). Likewise, the current also controls the relative abundance of gas in the system (influx). An examination of the amperometric responses shows similar currents across the experimental conditions at 0.05 CMC (**Figure S3**). Ultimately, the dynamic nature of the bubble radius of curvature, size, and shape is unknown. For example, a recent molecular simulation study challenged the stationary state (size) assumption of surface

nanobubbles at nanoelectrodes.[33] Notably, the majority of fluorophore labeling events range between 0.05-2 s on the bubble surface, and the fluorescent output, even in the repulsive fluorophore/surfactant condition, can exhibit similar behavior across various conditions. Thus, we speculate that the wide range of fluorophore interactions is indicative of a heterogeneous population of surface nanobubbles. Bubbles of different size and shape may also influence how the dye molecule interacts at the interface. Consequently, the thermodynamic landscape for fluorophore adsorption may change as a function of the physical properties of surface nanobubbles (contact angle, lateral vs longitudinal size, internal pressure, etc.). Additionally, the continued adsorption and desorption of surfactants will dynamically affect the contact angle at the surface nanobubble as the surface tension at the gas-liquid interface changes.[40] In other words, the interface is likely constantly changing/rearranging as different molecules come and go from the surface. Indeed, a greater control of the structural bubble features is needed to rule out any confounding factors affecting fluorophore/molecule adsorption at the interface. We are exploring the use of AFM coupled with spectroscopy to probe the structural effects in more detail.

Effect of surfactant on nanobubble labeling.

The unusual nanobubble labeling due to unfavorable electrostatics at a surfactant modified surface nanobubble is difficult to study in greater details using the present technique. As mentioned previously, the low intensity and transient nature of the adsorption/desorption phenomenon makes it challenging to define "spots" even when increasing the laser power (40 mW) or sampling at a faster camera frame rate (10 ms). Hence, the remainder of our study will be using favorable fluorophore-surfactant combinations (opposite charge).

Figure 3B shows a comprehensive surfactant concentration study for SDS and 16TAB using the appropriate dye molecule. First, it is worth mentioning that there is a noticeable difference in R6G and SRG lifetime without surfactant in solution (clean nanobubbles). We rationalize that this is likely due to a partial negative charge at the gas-liquid interface. Although a topic of debate, a negative charge at the gas-water interface may be possible due to the preferential orientation of water molecules or adsorbed hydroxide groups.[5,6,41] Recently, this plausible charge effect at the interface has been suggested to

partially explain a fluorophore concentration enhancement at the water-oil interface in aqueous microdroplets.[42,43] It is not clear whether this natural orientation of water molecules is present in our nanobubble experiments. However, in our study, the reduction of water to produce gaseous H_2 also produces abundant free hydroxides. As the nanobubbles are confined to the surface, we believe that there is a local excess concentration of hydroxide species available for adsorption to the bubble surface. This may result in slightly altered fluorophore adsorption at a "clean" nanobubble surface in the case of positively and negatively charged R6G and SRG molecules. Interestingly, adding 25 mM phosphate buffer (pH 7) does not cause significant changes to the measured residence time for SRG on the nanobubble surface, suggesting that that the buffer strength was insufficient to significantly alter the local chemical environment near the electrode surface. Although experimental and theoretical studies have demonstrated significant pH changes at the electrode surface during HER[44,45], buffer action functions well several microns away from the electrode surface[46]. Nonetheless, the true surface pH (nanometers from the electrode surface) remains high even under significant buffering conditions.[47] As surface nanobubbles exist within tens of nanometers from the electrode surface, our experimental observations seem appropriate when considering the ineffectiveness of the phosphate buffer to alter the SRG lifetime.

The fluorophore lifetime in the R6G-SDS condition increases dramatically from 55 ms to 90 ms at the lowest surfactant concentration and then reaches an apparent plateau around 100 ms with further surfactant addition (**Figure 3B**). We hypothesized that the plateau results due to a finite amount of surfactant adsorption sites on the nanobubble surface.[28] Thus, adding more surfactants does not alter how the fluorophore interacts. A similar effect was observed for single surface nanobubbles at a nanoelectrode.[19] Nonetheless, these results suggest that a thin layer of surfactant molecules is present along the bubble surface. Here we assume that a multi-layer surfactant structure is not present at the bubble surface due to unfavorable arrangement caused by the charged head groups. Yet, we previously suggested that a neutral surfactant, Triton X-100, may form dense, multi-layer aggregates at the bubble surface.[28]

On the other hand, there appears to be a significant difference in fluorophore lifetime in the SRG-16TAB condition (**Figure 3B**). We do not detect any changes in the extent of SRG labeling until roughly 0.01 CMC. The fluorophore lifetime continues to increase to 45 and 85 ms at 0.02 and 0.05 CMC, respectively. This result is surprising as 16TAB is generally considered more hydrophobic than SDS. Hence, we expected more 16TAB molecules to be present at the gas-liquid interface. Here we presume that more surfactant molecules at the interface yields extended fluorophore residence lifetimes. Alternatively, there may not be a significant amount of 16TAB molecules present on the bubble surface due to the lower absolute concentration of 16TAB in solution. The absolute concentration at 0.01 CMC 16TAB is 9.6 μM compared to 83 μM at 0.01 CMC SDS (**Table S1**). Nonetheless, a non-linear relationship between concentration and adsorption of surfactant to a surface nanobubble may exist.

The low-surfactant bulk concentration hypothesis to explain the extent of SRG-16TAB falls short when considering the fluorophore interactions at different cationic surfactants. **Figure 4** shows the effect of SRG lifetime at quaternary ammonium cationic surfactants of different carbon chain lengths. The presence of myristyltrimethylammonium bromide (14TAB) and dodecyltrimethylammonium bromide (12TAB) in solution appears to have little, if any, significant effect on SRG labeling. This result is unusual when considering the absolute concentrations of 16, 14, 12TAB. There is roughly 5 and 15 times more 14TAB and 12TAB at any given percent CMC when compared to 16TAB (**Table S1**). Therefore, the abundance of surfactant to adsorb at the nanobubble surface does not account for lack of change in fluorophore lifetime at the gas-liquid interface. It is likely that the charge on the CTAB molecule is close to zero due to the high local pH and excess OH^- ions produced from the water reduction reaction. In this situation, the entire CTAB molecule is more or less a neutral species. It is possible that there is an energy barrier for a close-to-neutral CTAB species to initiate its surface adsorption at the charged bubble surface. The reduction in the hydrophobic chain length may further reduce effective molecular adsorption and insertion of surfactants on bubble surface, i.e., the smaller 12TAB molecules may have a hard time inserting themselves into the gas/water interface. Therefore, it is expected that the total change in the surface charge due to surface adsorption of the TAB species is less significant than that from the SDS. As

such, the negatively charged SRG should experience a net repulsive force from the negative bubble surface leading to a reduced residence time.

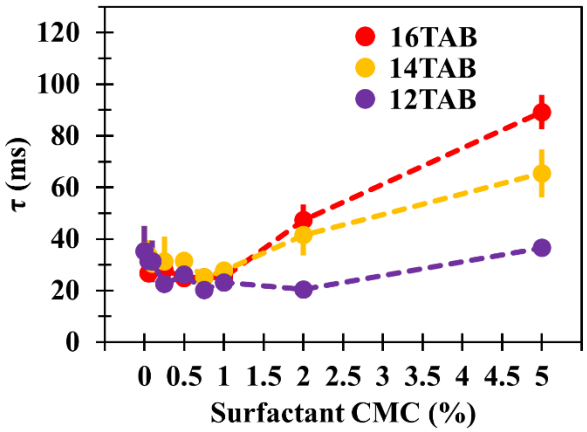

Figure 4: Effect of chain length on nanobubble labeling with SRG. Average SRG residence lifetime at a TAB stabilized nanobubble using 16-, 14-, and 12- carbon chain quaternary ammonium surfactants. All solutions contained 100 pM SRG, 1 M Na_2SO_4, and the appropriate surfactant type and concentration. N=5 for each condition. Error bars represent one standard deviation from the mean.

Ultimately, we believe the difference in SRG labeling of TAB modified nanobubbles can be explained when considering the relationship between fluorophore and surfactant adsorption/desorption at the bubble surface. In a surfactant containing solution, an equilibrium is quickly established between the concentration of surfactant species freely diffusing in bulk and those adsorbed on the bubble surface. This equilibrium results in a steady concentration of surfactant on a bubble surface. A similar equilibrium is established between the freely diffusing fluorophores, e.g., R6G, and those transiently adsorbed onto the bubble surface. A major difference, however, has to do with the exact surface concentrations of surfactant and the fluorophore. Due to the use of high concentration of surfactant, e.g., µM, and their relatively higher affinity to the gas/water interface, it is expected that there is a constant number of surfactant molecules on each bubble at any given time. On the other hand, a nanobubble will either have zero or one fluorophore molecule on its surface due to the very low concentration (pM) used in this study. Therefore, it is anticipated that the resident time of a fluorophore molecule on a bubble surface will be affected by the number of surfactant molecules on the same bubble surface and their charge state. The resident

lifetime of the surfactant on the bubble surface dictates the absolute concentration on the surface. We suggest that the less hydrophobic nature of 12 and 14-TAB yields smaller resident lifetimes at the bubble surface than in the 16-TAB condition. This decrease in surfactant lifetime yields a smaller absolute concentration on the bubble surface at any given time. Thus, the unchanged τ values indicate that the fluorophore adsorbs to a "cleaner" nanobubble in the case of 12 and 14-TAB.

Nevertheless, we hope our interpretation of a "clean" nanobubble does not skew the readers' perception of the physical landscape at the bubble surface. For us to observe a "spot", the concentration of fluorophore at the surface must be a single fluorophore. This does not necessarily mean that there are zero surfactant molecules at the gas-liquid interface. The physical meaning could imply that there are not enough surfactant molecules at any given time to affect fluorophore kinetics. In other words, we do not know how many surfactant molecules are required at the bubble surface to detect a lifetime change (τ) in a single fluorophore. Furthermore, we do not know the location of the fluorophore on the bubble surface when it "lights up". Consequently, an unchanged τ value in the presence of surfactant may indicate that the fluorophore is not labeling a surfactant rich region on the bubble. The distribution, orientation, and interfacial structure of surfactant on the surface of a nanobubble is unknown. We appreciate that elucidating these details is challenging but necessary to gain a better understanding of fluorophore-surfactant interactions at the gas-liquid interface.

Effect of salt on fluorophore adsorption.

The adsorption of anionic and cationic surfactants at the bubble surface requires ion pairing to maintain electroneutrality. Furthermore, the possibility of having a negatively charged bubble due to surface hydroxide groups will also require ion pairing even in the absence of charged surfactant. Hence, we hypothesized that the salt concentration and type may influence how fluorophores interact at the bubble surface.

Figure 5A shows fluorophore lifetime experiments using varying concentrations of Na_2SO_4 at SDS modified nanobubbles. Interestingly, we observe a decrease in lifetime across all surfactant concentrations as the salt concentration decreases. This result is somewhat unexpected because we

rationalized that decreasing the salt concentration would increase the attractive forces due to a decrease in charge screening at the bubble surface. Thus, the positively charged fluorophore would be more attracted to the negatively charged gas-liquid interface. However, changing the salt concentration affects the relative distribution of ions within the electric double layer at the ITO electrode itself. At 0.001 M Na_2SO_4 the double layer thickness is on the order of 20 nanometers.[48] As bubbles can exist within this size range, we believe that the negatively charged SDS molecules "feel" an increased repulsive electrostatic force from the ITO electrode that ultimately prevents adsorption to the bubble surface. Hence, the fluorophore adsorbs to a "clean" nanobubble surface. The electrostatic hindrance is partially overcome as the salt concentration increases to 0.1 M Na_2SO_4 due to an increase in electrode charge screening. This hypothesis is further supported when considering the number of bubbles detected at the various salt concentrations. Surfactants lead to the production of more surface nanobubbles due to a lowering of the gas concentration required for bubble nucleation.[28] **Figure S4** shows that the number of bubbles in the high salt condition is much different than without surfactant. The number of detections decreases to the R6G control value with decreasing salt. SDS molecules are not able to come close to the interface to assist in bubble nucleation. We observe a similar result when using the SRG-TAB system in low salt conditions as it becomes difficult for the negatively charged dye to approach the bubble surface due to an electric field influence from the electrode. The effect is partially overcome at high TAB conditions (i.e., 5% CMC 16TAB). Consequently, a nanobubble detection regime without the influence of electrochemistry is needed to determine the effect of salt concentration on single molecule interactions at a surface nanobubble.

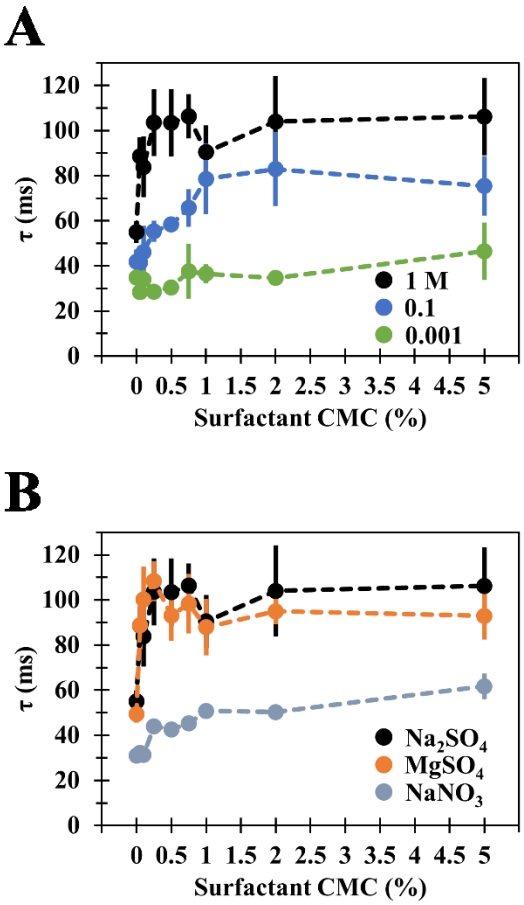

Figure 5: Effect of salt on nanobubble labeling. **A)** Average R6G residence lifetime at a SDS stabilized nanobubble using 1 M, 0.1 M, and 0.001 M Na_2SO_4 as the supporting electrolyte. **B)** R6G residence lifetime at a SDS stabilized nanobubble using 1 M Na_2SO_4, $MgSO_4$, and $NaNO_3$ as the supporting electrolyte. All solutions contained 100 pM R6G in addition to the appropriate salt and SDS concentrations. N=5 for each condition. Error bars represent one standard deviation from the mean.

Lastly, we studied the effect of different cation and anion salt species at the bubble surface. With electrostatic interaction in mind, we elected to vary the adsorbing cation (Na^+ vs Mg^{2+}) and anion (SO_4^{2-} vs NO_3^-) species as we hypothesized that their presence and charge (magnitude) would influence dye adsorption at the gas-liquid interface. There is no significant difference in fluorophore lifetime when using Na_2SO_4 or $MgSO_4$ as the supporting electrolyte (**Figure 5B**). However, the fluorophore interaction at the bubble surface is short lived in the $NaNO_3$ condition relative to Na_2SO_4 and $MgSO_4$ (**Figure 5B**). Presumably, the effect results due to a difference in the anionic species, SO_4^{2-} and NO_3^-. Yet, we are faced with the proverbial chicken-and-egg problem. Does NO_3^- affect R6G labeling or does NO_3^- affect SDS

adsorption? We believe that NO_3^- changes R6G bubble labeling as there is a substantial difference in the fluorophore lifetime in the Na_2SO_4 and $NaNO_3$ condition without the presence of surfactant (**Figure 5B**). Hence, some unknown property of the NO_3^- ion changes how the fluorophore interacts with the bubble surface even on a "clean" nanobubble. Briefly, the effect may be related but not limited to anion charge, size, surface distribution/concentration, or structural arrangement at the gas-liquid interface. The present report is not equipped to provide a more detailed explanation as the behavior and effect of nitrate at the interface is complex and illusive.[49]

Conclusions

In conclusion, the main takeaway from this work is that electrostatics appear to play an important role in single molecule adsorption at the gas-liquid interface. The fluorescent images and corresponding lifetimes change dramatically as a function of fluorophore and surfactant charge. Opposite charge fluorophore surfactant interactions (R6G-SDS and SRG-16TAB) lead to much longer lifetimes at surface nanobubbles in comparison to same charge conditions (R6G-16TAB and SRG-SDS). In general, single fluorophore residence on the nanobubble surface is a function of how many surfactants are adsorbed onto bubble; the more surfactant on the bubble the more likely that an observable change is detected. Once again, the change in the fluorophore lifetime, increase or decrease, is dictated by the attractive or repulsive nature of the gas-liquid interface relative to the dye. In a broader sense, we believe these results can be useful when evaluating the details of reactions at the gas-liquid interface as reactant, intermediate, and product molecule adsorption is conceivably governed by electrostatics at the interface; consequently, reaction rates and pathways may be influenced as well.

Furthermore, we demonstrated that the SRG molecules differ when labeling cationic surfactants of different carbon chain lengths. We hypothesized that a difference in surfactant equilibrium for the bubble surface relative to bulk liquid influences the surface concentration at any given time available to impact fluorophore labeling. Yet, we also rationalized that surfactant surface distribution on the bubble may play a role in the extent of fluorophore interaction as it is not clear where the labeling molecule lands

on the bubble surface. A procedure to monitor the relative location and lifetime of both surfactants and dye molecules would prove extremely useful for answering some of the lingering questions posed in this work. Therefore, we are exploring experimental setups that use fluorescent surfactants and dyes with distinct excitation and emission spectra to co-localize adsorption to the nanobubbles.

Additionally, we studied the effect of salt concentration and type on fluorophore labeling at the gas-liquid interface. Salt concentration studies showed that both fluorophores and surfactants become influenced by the electrical field at the working electrode as salt concentration decreases. Thus, this aspect of our report limits our ability to accurately evaluate the effect of salt concentration at surface nanobubbles. A methodology to study single molecules at surface nanobubbles without an applied electrical field is desirable. We demonstrated that salt type impacts the extent of fluorophore residence at bubble surface presumably due to differences in cation and anion chemical/physical properties and structural organization at the interface.

We leave the reader with several questions to reflect on. How does the radius of curvature, shape, and size of a surface nanobubble change the thermodynamic landscape for single molecule adsorption? Is the gas-liquid interface at a surface nanobubble structurally different than at a macroscopic interface? Does the influx and outflux of gas molecules influence how molecules come and go from the nanobubble surface? What are the major factors governing multi-molecule adsorption to surfactant modified nanobubbles? Answering these questions will continue to advance our understanding of the gas-liquid interface at a surface nanobubble.

Acknowledgement

This research was supported by the National Science Foundation (CHE-1904426).

Associated Content

Supporting information

Video imaging nanobubble labeling, table detailing surfactant concentrations, fluorophore structures, nanobubble detections at open circuit potential (-1V), time-current traces, nanobubble detections at different salt concentrations, labeling frequency, and single exponential decay fitting.

Notes

The authors declare no conflict of interest.

References

(1) Ruiz-Lopez, M. F.; Francisco, J. S.; Martins-Costa, M. T. C.; Anglada, J. M. Molecular Reactions at Aqueous Interfaces. *Nat. Rev. Chem.* **2020**, *4*, 459–475. https://doi.org/10.1038/s41570-020-0203-2.

(2) Kitanosono, T.; Kobayashi, S. Reactions in Water Involving the "On-Water" Mechanism. *Chem. - A Eur. J.* **2020**, *26*, 9408–9429. https://doi.org/10.1002/chem.201905482.

(3) Narayan, S.; Muldoon, J.; Finn, M. G.; Fokin, V. V.; Kolb, H. C.; Sharpless, K. B. "On Water": Unique Reactivity of Organic Compounds in Aqueous Suspension. *Angew. Chemie - Int. Ed.* **2005**, *44*, 3275–3279. https://doi.org/10.1002/anie.200462883.

(4) Lee, J. K.; Walker, K. L.; Han, H. S.; Kang, J.; Prinz, F. B.; Waymouth, R. M.; Nam, H. G.; Zare, R. N. Spontaneous Generation of Hydrogen Peroxide from Aqueous Microdroplets. *Proc. Natl. Acad. Sci.* **2019**, *116*, 19294–19298. https://doi.org/10.1073/pnas.1911883116.

(5) Björneholm, O.; Hansen, M. H.; Hodgson, A.; Liu, L. M.; Limmer, D. T.; Michaelides, A.; Pedevilla, P.; Rossmeisl, J.; Shen, H.; Tocci, G.; et al. Water at Interfaces. *Chem. Rev.* **2016**, *116*, 7698–7726. https://doi.org/10.1021/acs.chemrev.6b00045.

(6) Agmon, N.; Bakker, H. J.; Campen, R. K.; Henchman, R. H.; Pohl, P.; Roke, S.; Tha, M.; Hassanali, A. Protons and Hydroxide Ions in Aqueous Systems. *Chem. Rev.* **2016**, *116*, 7642-7672. https://doi.org/10.1021/acs.chemrev.5b00736.

(7) Jungwirth, P.; Tobias, D. J. Specific Ion Effects at the Air / Water Interface. *Chem. Rev.* **2006**, *106*, 1259–1281. https://doi.org/10.1021/cr0403741.

(8) Karakashev, S. I.; Nguyen, A. V.; Miller, J. D. Equilibrium Adsorption of Surfactants at the Gas-Liquid Interface. *Adv. Polym. Sci.* **2008**, *218*, 25–55. https://doi.org/10.1007/12_2008_161.

(9) Peng, M.; Nguyen, A. V. Adsorption of Ionic Surfactants at the Air-Water Interface: The Gap between Theory and Experiment. *Adv. Colloid Interface Sci.* **2020**, *275*, 102052. https://doi.org/10.1016/j.cis.2019.102052.

(10) Wang, L.; Wang, X.; Wang, L.; Hu, J.; Wang, C. L.; Zhao, B.; Zhang, X.; Tai, R.; He, M.; Chen, L.; et al. Formation of Surface Nanobubbles on Nanostructured Substrates. *Nanoscale* **2017**, *9*, 1078–1086. https://doi.org/10.1039/c6nr06844h.

(11) Wang, S.; Zhou, L.; Wang, X.; Wang, C.; Dong, Y.; Zhang, Y.; Gao, Y.; Zhang, L.; Hu, J. Force Spectroscopy Revealed a High-Gas-Density State near the Graphite Substrate inside Surface Nanobubbles. *Langmuir* **2019**, *35*, 2498–2505. https://doi.org/10.1021/acs.langmuir.8b03383.

(12) Wei, H.; Wang, H.; Tang, H.; Li, Y. Voltammetric Analysis of Single Nanobubble Formation on Ag and Ag@MoS 2 Nanoelectrodes . *J. Phys. Chem. C* **2021**, *125*, 3073–3080. https://doi.org/10.1021/acs.jpcc.0c10928.

(13) Ren, H.; Edwards, M. A.; Wang, Y.; White, H. S. Electrochemically Controlled Nucleation of

Single CO 2 Nanobubbles via Formate Oxidation at Pt Nanoelectrodes . *J. Phys. Chem. Lett.* **2020**, *11*, 1291–1296. https://doi.org/10.1021/acs.jpclett.9b03898.

(14) Theodorakis, P. E.; Che, Z. Surface Nanobubbles: Theory, Simulation, and Experiment. A Review. *Adv. Colloid Interface Sci.* **2019**, *272*, 101995. https://doi.org/10.1016/j.cis.2019.101995.

(15) Ranaweera, R.; Luo, L. Electrochemistry of Nanobubbles. *Curr. Opin. Electrochem.* **2020**, *22*, 102–109. https://doi.org/10.1016/j.coelec.2020.04.019.

(16) Tan, B. H.; An, H.; Ohl, C. D. Identifying Surface-Attached Nanobubbles. *Curr. Opin. Colloid Interface Sci.* **2021**, *53*, 101429. https://doi.org/10.1016/j.cocis.2021.101429.

(17) Tan, B. H.; An, H.; Ohl, C.-D. Stability of Surface and Bulk Nanobubbles. *Curr. Opin. Colloid Interface Sci.* **2021**, *53*, 101428. https://doi.org/10.1016/j.cocis.2021.101428.

(18) Zhang, X. H.; Maeda, N.; Craig, V. S. J. Physical Properties of Nanobubbles on Hydrophobic Surfaces in Water and Aqueous Solutions. *Langmuir* **2006**, *22*, 5025–5035. https://doi.org/10.1021/la0601814.

(19) Chen, Q.; Luo, L.; Faraji, H.; Feldberg, S. W.; White, H. S. Electrochemical Measurements of Single H2 Nanobubble Nucleation and Stability at Pt Nanoelectrodes. *J. Phys. Chem. Lett.* **2014**, *5*, 3539–3544. https://doi.org/10.1021/jz501898r.

(20) Wang, Y.; Chen, J.; Jiang, Y.; Wang, X.; Wang, W. Label-Free Optical Imaging of the Dynamic Stick-Slip and Migration of Single Sub-100-Nm Surface Nanobubbles: A Superlocalization Approach. *Anal. Chem.* **2019**, *91*, 4665–4671. https://doi.org/10.1021/acs.analchem.9b00022.

(21) Zhou, L.; Wang, X.; Shin, H. J.; Wang, J.; Tai, R.; Zhang, X.; Fang, H.; Xiao, W.; Wang, L.; Wang, C.; et al. Ultrahigh Density of Gas Molecules Confined in Surface Nanobubbles in Ambient Water. *J. Am. Chem. Soc.* **2020**, *142*, 5583–5593. https://doi.org/10.1021/jacs.9b11303.

(22) Wang, Y.; Gordon, E.; Ren, H. Mapping the Nucleation of H_2 Bubbles on Polycrystalline Pt via Scanning Electrochemical Cell Microscopy. *J. Phys. Chem. Lett.* **2019**, *10*, 3887–3892. https://doi.org/10.1021/acs.jpclett.9b01414.

(23) Lemineur, J.-F.; Ciocci, P.; Noël, J.-M.; Ge, H.; Combellas, C.; Kanoufi, F. Imaging and Quantifying the Formation of Single Nanobubbles at Single Platinum Nanoparticles during the Hydrogen Evolution Reaction. *ACS Nano* **2021**. *15*, 2643-2653. https://doi.org/10.1021/acsnano.0c07674.

(24) Chan, C. U.; Ohl, C. D. Total-Internal-Reflection-Fluorescence Microscopy for the Study of Nanobubble Dynamics. *Phys. Rev. Lett.* **2012**, *109*, 1–5. https://doi.org/10.1103/PhysRevLett.109.174501.

(25) Hain, N.; Handschuh-Wang, S.; Wesner, D.; Druzhinin, S. I.; Schönherr, H. Multimodal Microscopy-Based Identification of Surface Nanobubbles. *J. Colloid Interface Sci.* **2019**, *547*, 162–170. https://doi.org/10.1016/j.jcis.2019.03.084.

(26) Zhang, L.; Zhang, Y.; Zhang, X.; Li, Z.; Shen, G.; Ye, M.; Fan, C.; Fang, H.; Hu, J. Electrochemically Controlled Formation and Growth of Hydrogen Nanobubbles. **2006**, *6*, 8109–8113. https://doi.org/10.1021/la060859f.

(27) Hao, R.; Fan, Y.; Howard, M. D.; Vaughan, J. C.; Zhang, B. Imaging Nanobubble Nucleation and Hydrogen Spillover during Electrocatalytic Water Splitting. *Proc. Natl. Acad. Sci.* **2018**, *115*, 5878–5883. https://doi.org/10.1073/pnas.1800945115.

(28) Suvira, M.; Zhang, B. Effect of Surfactant on Electrochemically Generated Surface Nanobubbles. *Anal. Chem.* **2021**, *93*, 5170–5176. https://doi.org/10.1021/acs.analchem.0c05067.

(29) Hughes, L. D.; Rawle, R. J.; Boxer, S. G. Choose Your Label Wisely: Water-Soluble Fluorophores Often Interact with Lipid Bilayers. *PLoS One* **2014**, *9*. https://doi.org/10.1371/journal.pone.0087649.

(30) Mukerjee, P.; Mysels, K. J. *Critical Micelle Concentrations of Aqueous Surfactant Systems*; 1971. pp. 51, 57, 106. https://doi.org/10.1016/0021-9797(72)90423-7.

(31) Ovesný, M.; Křížek, P.; Borkovec, J.; Švindrych, Z.; Hagen, G. M. ThunderSTORM: A Comprehensive ImageJ Plug-in for PALM and STORM Data Analysis and Super-Resolution Imaging. *Bioinformatics* **2014**, *30*, 2389–2390. https://doi.org/10.1093/bioinformatics/btu202.

(32) Tinevez, J. Y.; Perry, N.; Schindelin, J.; Hoopes, G. M.; Reynolds, G. D.; Laplantine, E.; Bednarek, S. Y.; Shorte, S. L.; Eliceiri, K. W. TrackMate: An Open and Extensible Platform for Single-Particle Tracking. *Methods* **2017**, *115*, 80–90. https://doi.org/10.1016/j.ymeth.2016.09.016.

(33) Perez Sirkin, Y. A.; Gadea, E. D.; Scherlis, D. A.; Molinero, V. Mechanisms of Nucleation and Stationary States of Electrochemically Generated Nanobubbles. *J. Am. Chem. Soc.* **2019**, *141*, 10801–10811. https://doi.org/10.1021/jacs.9b04479.

(34) Brenner, M. P.; Lohse, D. Dynamic Equilibrium Mechanism for Surface Nanobubble Stabilization. *Phys. Rev. Lett.* **2008**, *101*, 1–4. https://doi.org/10.1103/PhysRevLett.101.214505.

(35) Liu, Y.; Edwards, M. A.; German, S. R.; Chen, Q.; White, H. S. The Dynamic Steady State of an Electrochemically Generated Nanobubble. *Langmuir* **2017**, *33*, 1845–1853. https://doi.org/10.1021/acs.langmuir.6b04607.

(36) Ma, Y.; Guo, Z.; Chen, Q.; Zhang, X. Dynamic Equilibrium Model for Surface Nanobubbles in Electrochemistry. *Langmuir* **2021**, *37*, 2771-2779. https://doi.org/10.1021/acs.langmuir.0c03537.

(37) Corzo, J.; Santamaria, M. Time, the Forgotten Dimension of Ligand Binding Teaching. *Biochem. Mol. Biol. Educ.* **2006**, *34*, 413–416. https://doi.org/10.1002/bmb.2006.494034062678.

(38) Lu, J.; Fan, Y.; Howard, M. D.; Vaughan, J. C.; Zhang, B. Single-Molecule Electrochemistry on a Porous Silica-Coated Electrode. *J. Am. Chem. Soc.* **2017**, *139*, 2964-2971. https://doi.org/10.1021/jacs.6b10191.

(39) Streubel, S.; Schulze-Zachau, F.; Weißenborn, E.; Braunschweig, B. Ion Pairing and Adsorption of Azo Dye/C16TAB Surfactants at the Air-Water Interface. *J. Phys. Chem. C* **2017**, *121*, 27992–28000. https://doi.org/10.1021/acs.jpcc.7b08924.

(40) Ducker, W. A. Contact Angle and Stability of Interfacial Nanobubbles. *Langmuir* **2009**, *25*, 8907–8910. https://doi.org/10.1021/la902011v.

(41) Vaécha, R.; Rick, S. W.; Jungwirth, P.; De Beer, A. G. F.; De Aguiar, H. B.; Samson, J. S.; Roke, S. The Orientation and Charge of Water at the Hydrophobic Oil Droplet - Water Interface. *J. Am. Chem. Soc.* **2011**, *133*, 10204–10210. https://doi.org/10.1021/ja202081x.

(42) Xiong, H.; Lee, J. K.; Zare, R. N.; Min, W. Strong Concentration Enhancement of Molecules at the Interface of Aqueous Microdroplets. *J. Phys. Chem. B* **2020**, *124*, 9938-9944. https://doi.org/10.1021/acs.jpcb.0c07718.

(43) Xiong, H.; Lee, J. K.; Zare, R. N.; Min, W. Strong Electric Field Observed at the Interface of Aqueous Microdroplets. *J. Phys. Chem. Lett.* **2020**, *11*, 7423–7428.

https://doi.org/10.1021/acs.jpclett.0c02061.

(44) Cannan, S.; Macklam, I. D.; Unwin, P. R. Three-Dimensional Imaging of Proton Gradients at Microelectrode Surfaces Using Confocal Laser Scanning Microscopy. *Electrochem. Commu.* **2002**, *4*, 886-892. https://doi.org/10.1016/S1388-2481(02)00482-4.

(45) Carneiro-Neto, E.B.; Lopes, M. C.; Pereira, E. C. Simulation of Interfacial pH Changes During Hydrogen Evolution Reaction. *J. Electroanal. Chem.* **2016**, *765*, 92-99. https://doi.org/10.1016/j.jelechem.2015.09.029

(46) Auinger, M.; Katsounaros, I; Meier, J. C.; Klemm, S. O.; Biedermann, P. U.; Topalov, A. A.; Rohwerder, M; Mayrhofer, K. J. Near-surface Ion Distribution and Buffer Effects During Electrochemical Reactions. *Phys. Chem. Phys. Chem.* **2011**, *13*, 16384-16394. https://doi.org/10.1039/C1CP21717H

(47) Ryu, J; Wuttig, A.; Surendranath, Y. Quantification of Interfacial pH Variation at Molecular Length Scales Using a Concurrent Non-Faradaic Reaction. *Angew. Chem. Int. Ed.* **2018**, *57*, 9300-9304. https://doi.org/10.1002/anie.201802756

(48) Bard, A. J.; Faulkner, L. R. Double-Layer Structure and Adsorption. In *Electrochemical Methods: Fundamentals and Applications*, 2nd ed.; John Wiley & Sons, Inc., 2001; pp 548-557.

(49) Hua, W.; Verreault, D.; Allen, H. C. Surface Electric Fields of Aqueous Solutions of NH_4NO_3, $Mg(NO_3)_2$, $NaNO_3$, and $LiNO_3$: Implications for Atmospheric Aerosol Chemistry. *J. Phys. Chem. C* **2014**, *118*, 24941–24949. https://doi.org/10.1021/jp505770t.

Table of Contents Figure